Journal of Materials Chemistry A

ROYAL SOCIETY OF CHEMISTRY

PAPER

View Article Online
View Journal

Cite this: DOI: 10.1039/d5ta06932g

Unexpected phase selectivity in germanosilicate zeolite synthesis: discovery and structure of HPM-18, a novel stable d4r-containing structure

Huajian Yu, [ab] Zhenghan Zhang,[c] Jian Li,[c] Salvador R. G. Balestra, [d] Zihao Rei Gao *[ae] and Miguel A. Camblor *[a]

For pure-silica zeolites containing double 4-ring (d4r) units, it is generally expected that zeolite solid solutions can form across the full range of Si–Ge compositions. This is because d4r units, although strained in pure-silica compositions, are stabilized by Ge atoms at their corners. In this work, we show that using 1,3,4-trimethylimidazolium and fluoride as structure-directing agents, the phase selectivity of crystallization shifts from zeolite ITW at pure-silica compositions to a new zeolite, HPM-18, at a low Ge fraction (0.15). HPM-18 contains the same d4r density as ITW and the same T-site fraction belonging to d4r, but is significantly more porous and less dense, making this phase selectivity change unexpected. Interestingly, while the structure of HPM-18 is ordered at a low Ge fraction, increasing the Ge fraction introduces two-dimensional correlated disorder, and up to five different ordered polymorphs can be identified in the resulting intergrowth materials. We report synthesis, structural characterization and energy minimization calculations that explain these findings. An energy penalty for Si/Ge substitution in ITW explains the phase selectivity change, while reduced energy differences between HPM-18 polymorphs in GeO_2 compositions account for the increased disorder as the Ge fraction increases.

Received 26th August 2025
Accepted 18th December 2025

DOI: 10.1039/d5ta06932g

rsc.li/materials-a

Introduction

Zeolites are crystalline microporous (alumino)silicates that find a wide range of applications in many industrial processes, including catalysis,[1] adsorption and separation processes,[2] and cation-exchange applications.[3] Their three-dimensional framework structures, composed of corner-sharing TO_4 tetrahedra (where T is typically Si or Al, but occasionally other atoms), contain pore systems with well-defined molecular dimensions due to the crystalline nature of zeolites. The properties of zeolites, typically high surface area, molecular sieving capabilities, cation exchange properties and tuneable acidity, enable them to outperform other materials in numerous applications that range from oil refining to gas adsorption/separation and environmental remediation.[4–8]

The synthesis of zeolites is a complex and still not well-understood process governed by many interacting factors, among which the use of the so-called organic structure-directing agents (OSDAs) typically plays a key role.[9] These organic molecules, frequently cations, interact with the inorganic species during crystallization, determining to some extent the final zeolite structure and ending up occluded in its pores and cages.[10] The concept of structure direction has been fundamental in furthering the development of zeolite science, allowing for the discovery of many new framework types and new zeolite compositions as well as for the optimization of existing zeolites for specific applications.[11] Inorganic structure-directing agents also exist. Among them, the use of some heteroatoms (T atoms other than silicon that can occupy tetrahedral framework positions) and fluoride (a catalyst for the breaking and formation of T–O–T bonds) is of particular importance. The incorporation of Ge into zeolite frameworks has opened up new possibilities in zeolite synthesis.[12] The larger Ge ionic radius and more flexible Ge–O–Ge angles compared to silicon allow for the stabilization of certain structural units, particularly double four-ring (d4r) units, which are strained in pure silica compositions.[13] The fluoride route, which involves the use of fluoride anions as mineralizing agents, has been particularly successful in enabling the synthesis of high-silica zeolites with reduced framework defects, including d4r structures, especially under highly concentrated conditions.[14,15] According to calculations by Zicovich Wilson and co-workers, occlusion of fluoride in d4r units makes the framework more flexible by decreasing the covalent character, and hence the

[a]Instituto de Ciencia de Materiales de Madrid (ICMM), CSICC/ Sor Juana Ines de la Cruz, 3, 28049 Madrid, Spain. E-mail: macamblor@icmm.csic.es

[b]Escuela de Doctorado, Universidad Autónoma de Madrid, Madrid 28049, Spain

[c]State Key Laboratory of Coordination Chemistry, School of Chemistry and Chemical Engineering, Nanjing University, Nanjing 210023, China

[d]Departamento de Física Atómica, Molecular y Nuclear, Área de Física Teórica, Universidad de Sevilla Av. Reina Mercedes s/n, 41012 Seville, Spain

[e]Department of Chemical and Biomolecular Engineering and Institute for NanoBioTechnology, Johns Hopkins University, 3400 N Charles St., Baltimore, MD 21218, USA. E-mail: zgao44@jhu.edu

directionality, of the Si–O bond.[16,17] This makes pure silica structures containing d4r units accessible for crystallization, despite their strained nature. Calcination of the zeolite removes the occluded fluoride, alongside the OSDA, and typically renders an essentially perfect, defect-free, SiO_2 framework.[18,19]

Although germanosilicates with high Ge content often exhibit limited hydrothermal stability, they remain of significant interest to researchers for two key reasons. Firstly, these materials can frequently be utilized in the assembly–disassembly–organization–reassembly (ADOR) process, leading to the creation of novel zeolitic materials with unique structural features and improved stability.[20–22] The ADOR process takes advantage of the chemical weakness in Ge-rich frameworks to selectively disassemble and then reassemble the structure, often resulting in new zeolite topologies that are unattainable through direct traditional synthesis routes.[23] Secondly, newly discovered structures that are first obtained as germanosilicates can serve as targets for the design of new organic structure-directing agents (OSDAs) that could potentially yield these frameworks in more stable, low-germanium high-silica compositions.[24] Thus, both approaches have the potential to expand the range of accessible zeolite structures while improving their stability and applicability. Additionally, post-synthesis methods can convert unstable germanosilicates into stable materials with lower Ge content.[25–27]

For pure-silica zeolite structures containing d4r units, such as ITW,[28] one could expect that it should be possible to prepare zeolite solid solutions across the entire range of Ge fractions (Ge_f = Ge/(Ge + Si) from 0 to 1) using the fluoride route. This expectation stems from the known affinity of both fluoride and germanium atoms for d4r units, which should in principle stabilize these structures across all Ge–Si compositions. This, for instance, has been shown to be the case for zeolite STW, also containing d4r, which we have synthesized in the whole range from pure silica to pure germania.[29,30] Examples with the AST framework type also exist.[31] However, in this work, we report a surprising finding that challenges the above assumption. Using 1,3,4-trimethylimidazolium (134TMI) as the OSDA and fluoride anions as mineralizing agents, *i.e.* the structure directing agents first used to discover ITW,[32] we observed a dramatic shift in phase selectivity from ITW to a new zeolite structure, designated as HPM-18 (zeolite number 18 from the Nanostructured Hybrid Biohybrid and Porous Materials group of ICMM, Madrid), at a remarkably low Ge fraction of just 0.15. Intriguingly, HPM-18 contains the same density of d4r units as ITW (one d4r per 12 T atoms) and an identical fraction of T sites belonging to d4r (2/3 of T sites). This unexpected change in phase selectivity at such a low germanium content is particularly perplexing, given the structural similarities between ITW and HPM-18 in terms of their d4r content. ITW possesses a relatively simple framework with a 2D system of pores defined by rings containing 8 $SiO_{4/2}$ tetrahedra, *i.e.* 8R pores, while the structure of HPM-18 is rather complex and less dense, featuring a rather intricate system of pores: 12R, 8R and 7R pores run along one crystallographic direction (*b*) while a second pore will be described below. Thus, HPM-18 is a new addition to the scarce "odd zeolites", *i.e.* those zeolites that contain odd-membered pores,[33] a class of zeolites that constitutes less than 5% of all the ordered zeolite framework types recognized by the Structure Commission of the International Zeolite Association.[34] HPM-18 contains, in fact, rings with all possible numbers of atoms from 4 to 12. Additionally, we show here that HPM-18 can also be synthesized with higher Ge_f and in that case we observe two dimensional correlated disorder, with up to five different polymorphs identified. Thus, it is only the third odd zeolite that can be a disordered intergrowth of different polymorphs, after EMM-17 and HPM-14.[35,36] These three intergrown odd zeolites possess different odd pores: 11R in EMM-17, 9R in HPM-14, and 7R in HPM-18.

Here, we present a comprehensive study of the synthesis, structural characterization, and energetics of HPM-18. Our aim, in addition to reporting a new zeolite structure, is to gain insights into the underlying factors driving this unexpected phase selectivity and to contribute to a deeper understanding of the complex interplay between composition, structure direction, and framework energetics in zeolite crystallization. This investigation not only introduces a novel zeolite but also challenges our current understanding of structure direction in germanosilicate zeolite synthesis, potentially contributing to the development of new strategies for the discovery of new zeolites.

Results and discussion

Zeolite synthesis and physicochemical characterization of HPM-18

In the absence of Ge, 134TMI structure-directs the crystallization of pure silica ITW,[32] although under certain conditions, TON may crystallize first and then recrystallize into the more porous and less stable (in the absence of guests) ITW.[37] This is a quite unique example of stability reversal by host–guest interactions. Among the three small imidazolium cations known to act as OSDAs for pure silica ITW, 134TMI has been rated as the worst OSDA.[17] When Ge is introduced in the crystallizing medium other phases start to compete (Table S1). For a $Ge_f = 0.1$, ITW still dominates the crystallization field but at the higher concentration tried ($H_2O/SiO_2 = 1$), some competition with HPM-18 already occurs. Upon further increasing the Ge_f the crystallization of HPM-18 is clearly favored, although a significant dependency on the water content is also observed. For instance at $Ge_f = 0.15$ we obtained pure HPM-18 at high concentrations and pure ITW at low concentrations (H_2O/SiO_2 = 2.5 and 6, respectively). A further increase in Ge_f to 0.2 favors HPM-18 *vs.* ITW and at 0.3 the competition is between HPM-18 (again favored at high concentrations) and a phase of the disordered IM-18 family.[38] The presence of IM-18, which can be detected by two sharp peaks around 7.7 and 15.7° and a broad one around 8.7°, is more prominent as the degree of dilution increases (Fig. S6).

At a Ge_f of 0.6 and 0.8 the only crystalline phase obtained is HPM-18 for any H_2O/SiO_2 ratio tried, while at a pure germanate composition, dense GeO_2 was obtained. These results clearly suggest that Ge favors HPM-18 *vs.* ITW or IM-18 and at low Ge_f, HPM-18 is favored at high concentrations. As derived from the

structural analysis below, the experimental framework density (FD, expressed in this paper always as T atoms per 1000 Å^3) of calcined HPM-18 (17.00 for a $Ge_f = 0.17$) is considerably lower than that of calcined ITW (18.15, $Ge_f = 0$)[28] and as-made 4-dimethylaminopyridine-IM-18 (17.85 for $Ge_f = 0.32$). Despite the fact that there certainly must be an influence of both Ge_f and the presence of occluded guests on the calculated FD, so that the above FDs are not directly and exactly comparable, we find it very likely that HPM-18 is the least dense of the three phases in question here. This suggests that our empirical observations agree with Villaescusa's rule, which was derived from observations of purely siliceous zeolite systems and states that, in fluoride media, the less dense phases are favored at higher concentrations.[14] The plausible applicability of the Villaescusa rule to germanosilicate zeolites has recently been proposed.[39]

Fig. 1 shows the PXRD patterns of HPM-18 synthesized from gels with Ge_f from 0.15 to 0.8. All the as-made materials show good crystallinity (Fig. 1a), while peak positions and relative intensities vary as the Ge_f changes. However, after calcination (Fig. 1b) samples with a Ge_f of 0.3 or higher show an evident structural degradation right after calcination. In contrast, for the sample with $Ge_f = 0.17$ the structural integrity is maintained even after exposure to ambient air for 6 days. Ar adsorption/desorption isotherms on the calcined sample revealed a specific surface area of 327 m^2 g^{-1} (Fig. S10) and the details are given in the SI.

According to ^{13}C MAS NMR (Fig. 2A) the OSDA is occluded intact in HPM-18. Chemical analysis suggests that there are around 4 cations per unit cell of HPM-18 in the sample with less Ge (Table 1) and that the zeolite also contains a large amount of water. The excess OSDA observed in Table 1 is attributed to the difficulty in washing away OSDA occluded in the intercrystallite space. The ^{19}F MAS NMR spectra of HPM-18 with different Ge_f values are shown in Fig. 2B. All the samples show resonances in the range expected for fluoride occluded in d4r cages. We note here that samples that are incompletely washed may show a sharp resonance around −120 to −130 ppm, likely related to fluoride in F–Si bonds. The samples with more Ge show a strong resonance around −10/−11 ppm, *i.e.* type III corresponding to fluoride in d4r containing Ge pairs but not larger Ge clusters. This type of d4r can have between 2 and 6 Ge atoms.[30] The sample with $Ge_f = 0.3$ also contains a second small signal around −21 ppm, *i.e.* type II, corresponding to d4r containing non-paired Ge (which may contain between 1 and 3 isolated Ge). By contrast, the sample with less Ge shows a type I resonance around −40 ppm as well as types II (−22 ppm) and III (−12 ppm). The ^{29}Si MAS NMR and ^{29}Si{^{1}H} CP are shown in Fig. 2C and are typical of germanosilicates with varying Ge_f. Cross-polarization enhances all the resonances at lower fields. After calcination only resonances in the −94/−120 ppm range are observed, as expected for germanosilicate zeolites (Fig. 2C, top).

cRED structure solution and Rietveld refinement of ordered calcined HPM-18 of Ge_f 0.17

cRED data processing was carried out with the XDS software package. To enhance data completeness, several selected datasets for each sample were rescaled and merged using XSCALE (within the XDS suite), producing HKL files for subsequent structure solution and refinement. Following cRED data acquisition, the 3D reciprocal lattice was reconstructed using REDp, which facilitated indexing and identification of reflection conditions. The structure of HPM-18 was initially solved from the cRED data of a sample with a very high Ge_f (0.8). However, we suspected an effect of Ge_f on disorder from an analysis of the broadness of the reflection peaks: determination of the fwhm of the 3.3° peak of the SPXRD patterns of four samples with varying Ge_f shows that the fwhm sharply increases when the Ge_f increases from 0.17 to 0.6 (60% increase) and then slightly decreases for $Ge_f = 0.8$ (Fig. S7). This occurs despite the fact that

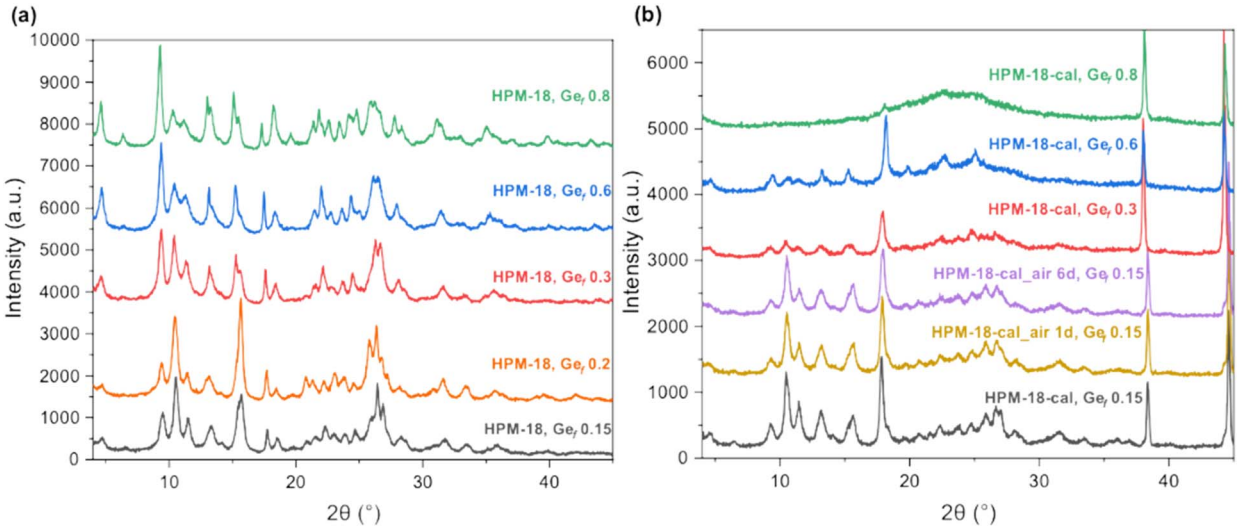

Fig. 1 PXRD patterns of (a) five as-made HPM-18 samples with different Ge_f values in gel (from bottom: 0.15, 0.2, 0.3, 0.6 and 0.8) and (b) calcined HPM-18 (from bottom to top: calcined HPM-18 (Ge_f 0.15), calcined HPM-18 exposed to ambient air for 1 day and 6 days; calcined HPM-18 (Ge_f 0.3) and calcined HPM-18 (Ge_f 0.6) respectively. Two peaks around 37.5° and 45° in (b) belong to the aluminum sample holder.

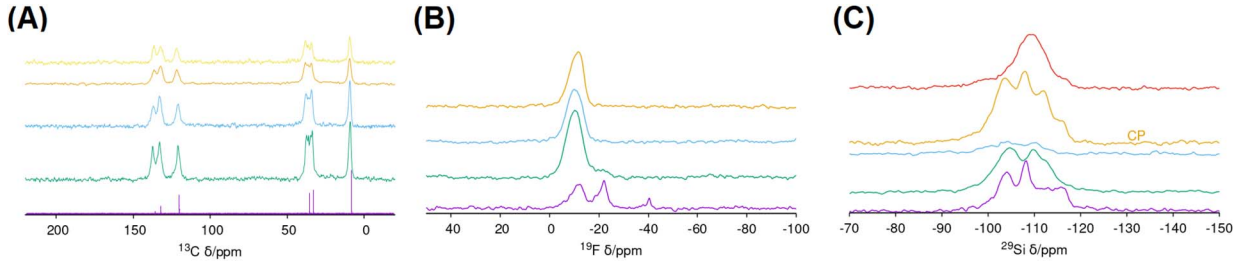

Fig. 2 MAS NMR study of HPM-18: (A) ^{13}C MAS NMR spectrum of HPM-18 with (from top) $Ge_f = 0.8$, 0.6, 0.3 and 0.17 and ^{13}C NMR in D_2O of 134TMI iodide (bottom); (B) ^{19}F MAS NMR spectra of HPM-18 samples synthesized from gels with $Ge_f = 0.1$ (bottom), 0.3, 0.6 and 0.8 (top); (C) ^{29}Si MAS NMR spectra of HPM-18 (from bottom) with $Ge_f = 0.17$, 0.3, 0.6 and ^{29}Si {^{1}H} CP MAS NMR of the sample with $Ge_f = 0.17$ and ^{29}Si MAS NMR spectrum of calcined HPM-18 ($Ge_f = 0.17$).

Table 1 Chemical composition of HPM-18

	wt%			Molar ratio[b]		wt%[c]	
Ge_f[a]	N	C	H	C/N	H/N	TG residue	Unit cell[d]
0.17	3.13	8.68	1.96	3.24	8.69	81.5 (79.0)	$(C_6N_2H_{11}F)_{4.59}(H_2O)_{14.64}[Si_{39.84}Ge_{8.16}O_{96}]$
0.35	3.29	8.53	1.74	3.03	7.34	82.7 (80.8)	$(C_6N_2H_{11}F)_{5.28}(H_2O)_{9.71}[Si_{31.2}Ge_{16.8}O_{96}]$
0.63	3.29	8.39	1.68	2.98	7.09	82.7 (81.3)	$(C_6N_2H_{11}F)_{6.11}(H_2O)_{9.71}[Si_{17.76}Ge_{30.24}O_{96}]$
0.78	3.07	7.65	1.53	2.91	6.93	84.0 (82.9)	$(C_6N_2H_{11}F)_{6.02}(H_2O)_{8.60}[Si_{10.56}Ge_{37.44}O_{96}]$

[a] By EDS. [b] The ratios in pristine134TMI are C/N = 3.0 and H/N = 5.5. [c] The value calculated for the composition in the last column appears between parentheses. [d] OSDAF calculated from the N content, water from the excess H.

the size of the crystallites tends to increase continuously with Ge_f (see Fig. S8). Hence, two additional samples ($Ge_f = 0.17$ and 0.6) were studied by cRED in order to investigate the influence on Ge on disorder. cRED showed the presence of streaks in the samples with higher Ge_f, indicative of disorder (Fig. S1–S3), but no streaks were detected in the sample with $Ge_f = 0.17$ (Fig. S4 and S5). For that sample, the structure of HPM-18 was determined *ab initio* using SHELXT, with the HKL file (containing reflection data) and P4P file (containing unit cell parameters) as inputs. This enabled direct localization of all framework atoms within the asymmetric unit, 24 T atoms and 48 O atoms. The final structure refinement was performed in Olex2 using electron-specific atomic scattering factors. Detailed crystallographic data obtained *via* cRED are provided in Tables S1 and S2. The same procedure applied to the initial dataset collected from the sample with higher Ge_f afforded a solution corresponding to the average structure of a zeolite exhibiting a large degree of correlated 2D disorder arising from two possible locations of four of the d4r units along the *b* direction (see below), of which the former ordered structure was a particular polymorph (polymorph D, see below).

An ordered polymorph model of HPM-18 with low Ge content was directly obtained from cRED data in P-1 (its maximum symmetry). This model was used as the initial structure for Rietveld refinement against synchrotron powder X-ray diffraction (SPXRD) data using Topas 5.0.[40] Prior to refinement, the framework geometry was optimized *via* the distance-least-squares (DLS) algorithm implemented in DLS-76,[41] and the SPXRD background was manually subtracted. In the initial refinement steps, soft restraints were applied to Si(Ge)–O bond lengths (1.61–1.72 Å), Si(Ge)–O–Si(Ge) angles (145°), and O–Si–O angles (109°). These restraints were gradually relaxed over several cycles. Additionally, the Si and Ge occupancies of each crystallographic T site were also refined, resulting in around 80% of the Ge being located in d4r units; details are provided in the SI. To account for anisotropic line broadening, a dedicated Topas macro contributed by Prof. Alan Coelho was employed.[42] The structure of ordered HPM-18 will be discussed below in relation to disorder and the pore system. Crystallographic Tables (S4–S6) and the Rietveld plot (Fig. S9) are provided in the SI and the cif file has been deposited in the CCDC database (CCDC 2476607).[43]

Topology analysis: disorder and polymorph extraction and HPM-18 structure description

In the average structure obtained from cRED of the highest Ge_f material there are four d4rs per unit cell with half occupancy and another two d4rs that are completely ordered (Fig. 3). Looking down [010], disorder is observed around positions A (0.25a, 0.25c), B (0.25a, 0.75c), C (0.75a, 0.25c) and D (0.75a, 0.75c). At each position, the d4r can be located either at the top ($b = 0.5$–1, marked as circle in Table S7) or at the bottom ($b = 0$–0.5, marked as crosses in Table S7) half of the unit cell. The top and the bottom positions are mutually exclusive, meaning that if the top space were occupied by a d4r, then the bottom space must remain unoccupied, and *vice versa*, resulting in correlated disorder. The unoccupied space is a cage occupied by the OSDAs in the as-made form of HPM-18. However, the sequence (top or bottom) of the d4r at one position does not determine

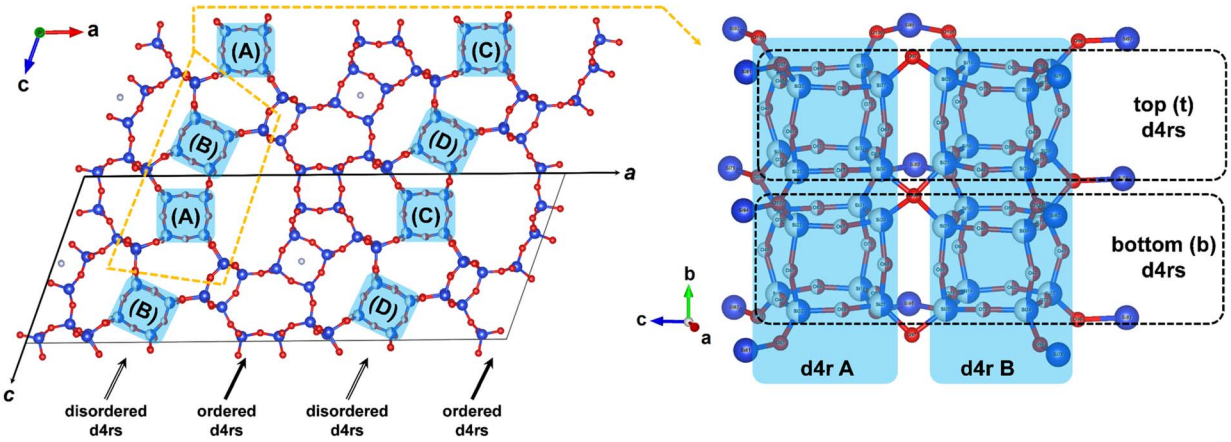

Fig. 3 Structure of HPM-18 with correlated disorder of four d4r units (highlighted in blue), viewed along the [010] direction, (left) and the top/bottom possible positions of d4r at positions A and B, viewed along approximately the [101] direction (right). The T and O atoms from the disordered d4r are shown as half-occupied blue and red spheres, respectively, while the other T sites and O atoms are depicted as fully occupied blue and red spheres. The structure on the right corresponds to the orange dashed frame on the left and the top and bottom positions are mutually exclusive.

the sequences at the other positions. This means that each unit cell has four independent variables determining the position of the d4rs. In other words, there are four independent possibilities controlling whether the d4r occupies the top or bottom position at each site (A to D). The disorder observed in HPM-18 at high Ge fractions is similar to that observed in IM-18,[44] CIT-13,[45] and NUD-2.[46] In IM-18 three simple ordered polymorphs could be derived: EOS (ECNU-16),[47] IM-18 polymorph B, and ITW.[48] In CIT-13 and NUD-2, three simple ordered polymorphs could also be derived. In HPM-18, a systematic exploration of all the possible polymorphs resulting from the $2^4 = 16$ possible combinations of disorder (two possible positions along *b* for each of the four A–D positions, see table S7) revealed that only five polymorphs are topologically distinct from each other, namely polymorphs A (with all four A–D positions at the top, *i.e.* tttt), B (with D at the bottom, tttb), C (C and D at the bottom, ttbb), D (B and D at the bottom, tbtb) and E (B and C at the bottom, tbbt).

Along the [010] direction, the five polymorphs of HPM-18 do not exhibit disorder, and the straight 12R, 8R, and 7R channels remain unblocked (Fig. 4a). These straight channels are "fused", meaning that adjacent channels share single Si–O–Si bonds, which would facilitate efficient diffusion of guest molecules from one set of channels to another. When viewed along the [001] direction, these five polymorphs possess different channel systems due to the presence of disorder. Polymorphs A, B, and C retain straight 10R channels, whereas in polymorphs D and E the 10R pores are blocked by the undulated d4r (Fig. 4b–f).

During the topology analysis, a large pocket-like tile $[4^7.5^6.7^2.8^2.12^2]$ was identified in all polymorphs A–E (Fig. 4g). These tiles (Fig. 4g) are rotated, shifted, connected through the 12R, and repeated every four tiles along the *b*-axis, forming the 12R channel shown in Fig. 4h. The stacking sequence is illustrated in Fig. 4j as red–orange–yellow–green stacking down along the *b*-axis. For instance, the red tile is rotated into the orientation of the orange tile with a $-1/4b$ shift. This combination of rotation and translation along the *b*-axis is repeated to build the structure shown in Fig. 4j. When Fig. 4j is viewed from

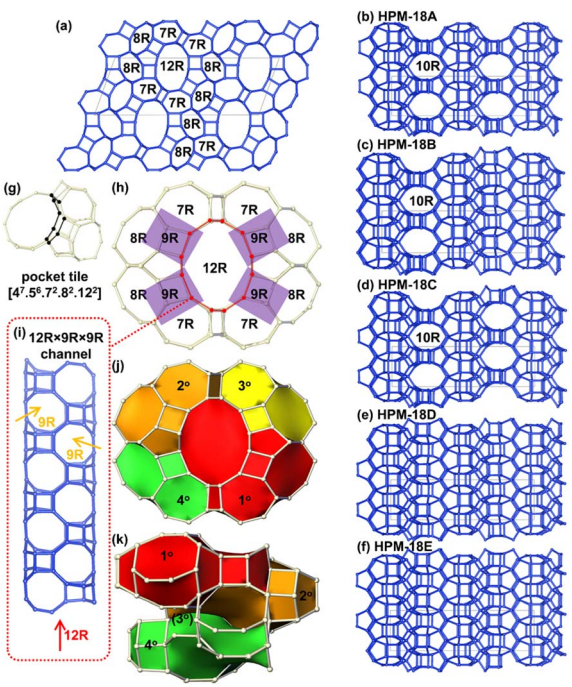

Fig. 4 Structure of HPM-18: (a) viewed along the [010] direction showing the straight 12R, 8R, and 7R channels; (b–f) HPM-18 polymorphs A–E viewed along the [001] direction, showing straight 10R in polymorphs A–C and the absence of straight 10R channels in polymorph D–E (where undulating 10R exist instead); (g) a large pocket-like tile [47.56.72.82.122] present in all polymorphs; (h) 4 pocket-like tiles; (i) straight 12R channels with 9R pore stretches opening to the 4 pockets, (j) stacking sequence of 4 pockets (red–orange–yellow–green) along the [010] direction; (k) view through the yellow pocket to show the 9R pore connecting the 12R and 8R channels.

another direction, with the yellow tile removed for clarity, the resulting structure is shown in Fig. 4k, revealing that 9R pore stretches exist at the intersections of the 12R straight channels and the pockets (Fig. 4i). Topology analysis also indicates that HPM-18 contains de facto rings with all possible numbers of atoms from 4 to 12. However, only 4R, 5R, 7R, 8R, and 12R are considered as "strong rings", *i.e.* they are rings that are not the sum of smaller rings. As a result, HPM-18E possesses a 3D 12 × 8 × 8 R channel system, with additional 7R and 8R channels aligned in the same direction as the 12R channel.

Site-occupancy disorder and stability of ITW and HPM-18

For each HPM-18 polymorph as well as for ITW we generated structures with full occupancies of T (as Si or Ge) and O sites, and the structures were energy-minimised. Table 2 shows the enthalpy results for the five polymorphs and ITW zeolites as SiO_2 and GeO_2 compositions. For pure silicate zeolites the most stable zeolite is ITW. The enthalpic order for the HPM-18 polymorphs is E > D > B > A > C, with relative enthalpies with respect to the most stable phase of 0.14 (D), 1.51 (B), 2.79 (A), and 2.81 (C) kJ mol^{-1}. Regarding GeO_2 compositions, all HPM-18 polymorphs are more stable than ITW. The stability order is the same as for SiO_2 compositions but with relative enthalpies of 0.19 (D), 0.66 (B), 1.17 (A), and 1.41 (C) kJ mol^{-1}. It is important to note, first, that the most stable HPM-18 polymorph, E, is the one that arose from the structural model obtained from cRED data at low Ge content, and also the one successfully used in the Rietveld refinement of that zeolite. Second, the energy span in Table 2 is much larger on the SiO_2 side (5.26 kJ mol^{-1}) than on the GeO_2 side (1.42 kJ mol^{-1}). Third, there is a significant energy penalty associated with the substitution of Si by Ge in ITW (over 4 kJ mol^{-1}), while in HPM-18 that substitution implies either a small penalty (0.02–0.88 kJ mol^{-1} for the most stable polymorphs) or a small benefit (−0.5 to −0.72 kJ mol^{-1} for the less stable polymorphs A and C). These calculations help to rationalise the observed structure-direction change from ITW to HPM-18 at low Ge fractions (due to the significant penalty of Si by Ge substitution in ITW), and they also indicate that the convergence of polymorph energies at high Ge content increases the relevance of entropic contributions, favouring disorder and intergrowth.

The energy minimisation calculations above provide insights into the relative thermodynamic stability of the five HPM-18 polymorphs and ITW, but they were performed for pure SiO_2 and GeO_2 compositions. Direct comparisons across compositions must therefore be interpreted with caution due to the differing chemical environments and bonding preferences of Si and Ge. A more rigorous approach involving enthalpies or formation energies for intermediate compositions could, in principle, provide a more complete view of the energetic landscape. For this reason, we have instead examined the evolution of the ensemble-averaged Gibbs energy, $\langle \Delta g \rangle$, with respect to the Ge fraction (Ge_f), primarily for the ITW and HPM-18 E frameworks across the full compositional range. To achieve this, we developed a modified version of the SOD code tailored to this system (see the SI). In addition, both OSDA cations and F^- anions were explicitly included in all energy optimisations, as detailed in the methodological section of the SI.

As shown in Fig. 5, introducing Ge into ITW stabilises the framework at very low Ge_f values, but leads to destabilisation at higher fractions (*ca.* $Ge_f \sim 0.2$) relative to the HPM-18-E framework. Although the HPM-18-E structure has a higher enthalpy than ITW, the increasing mixing entropy as Ge_f increases, together with an additional configurational contribution associated with polymorphism (*ca.* −5.45 and −5.62 kJ mol^{-1} for the $Ge_f = 0$ and $Ge_f = 1$ values, respectively), results in a substantial decrease in Gibbs energy and enhances the stability of the polymorph mixture. This polymorph entropy corresponds to the configurational contribution arising from the number of distinct polymorphs accessible at a given Ge_f, as detailed in the SI. So, when the configurational entropy is incorporated into the analysis, the thermodynamic picture becomes fully consistent

Table 2 Calculated enthalpy per T-atom with respect to SiO_2 or GeO_2 quartz, Δh, for HPM-18 polymorphs and ITW zeolites. In bold numbers, we have highlighted the most stable zeolite for SiO_2 and GeO_2 compositions

	Δh/[kJ mol^{-1}]	
	SiO_2	GeO_2
HPM-18A	14.02	19.23
HPM-18B	12.71	18.71
HPM-18C	14.00	19.47
HPM-18D	11.34	18.24
HPM-18E	11.20	18.05
ITW	8.76	18.82
Span ($\Delta\Delta h$)[a]	5.26	1.42

[a] Span ($\Delta\Delta h$) is the enthalpy difference between the highest and lowest calculated energies in each column.

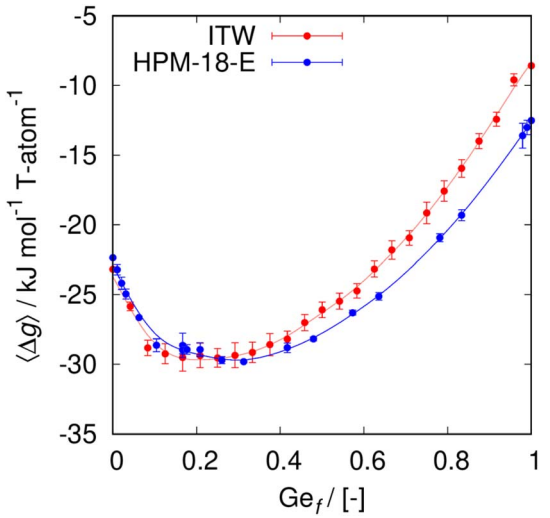

Fig. 5 Calculated $\langle \Delta g \rangle$ ensemble-averaged Gibbs energies per T-atom relative to a linear combination of quartz SiO_2 and quartz-type GeO_2 (for $Ge_xSi_{1-x}O_2$ compositions) at 150 °C, and hypothetical 134TMI$^+$F-salt, for ITW (red) and HPM-18 E (blue) zeolites. See the SI for the estimation of error bars. Solid lines represent spline interpolations of the free energy data, included solely to guide the eye.

with the experimentally observed disorder: as the polymorphs approach energetic degeneracy at high Ge content, the system favours disordered intergrowths that maximise configurational entropy, manifested experimentally as streaks in cRED data and peak broadening in PXRD patterns.

These results reinforce the conclusions obtained from the enthalpy analysis and help explain why the phase selectivity of the crystallisation shifts from ITW to HPM-18 at relatively low Ge contents. In addition, vibrational entropy may contribute to the overall disorder and the evolution of phase selectivity, although the present analysis accounts only for the configurational component (mixing and polymorph entropies). Vibrational effects are expected to be smaller in magnitude but could further modulate the free-energy balance, particularly at elevated temperatures.

Conclusions

In this work, we report the discovery and structural characterization of HPM-18, a novel germanosilicate zeolite featuring double four-ring (d4r) units and an unusual phase selectivity behavior in its synthesis. Contrary to our expectations based on previous structure-directing observations, the use of 1,3,4-trimethylimidazolium (134TMI) and fluoride ions led to the crystallization of HPM-18 at a low Ge fraction ($Ge_f = 0.15$ in the gel), instead of the anticipated denser ITW phase, while ITW is the predominant phase at pure silica compositions. This finding challenges the assumption that d4r-containing frameworks like ITW should be favored across the full Ge–Si compositional range under fluoride-mediated conditions. The structure of HPM-18 has been solved from cRED data. It exhibits a complex pore system containing both even and odd-membered rings and can be synthesized over a wide range of Ge contents. However, while at very low Ge_f the structure is ordered and coincides with the most stable polymorph E, at high Ge fractions the structure displays two-dimensional correlated disorder, resulting in an intergrowth of multiple possible polymorphs. The ordered structure has been Rietveld refined using SPXRD. HPM-18 has a lower framework density than ITW and IM-18 and is favored at high concentrations, consistent with the empirical Villaescusa's rule, which correlates phase selectivity with framework density and concentration in fluoride media. Calculations suggest a large penalty for substituting Si with Ge in ITW, which accounts for the observed structure-direction change at low Ge_f. They also indicate that the six HPM-18 polymorphs become increasingly similar in energy as the Ge content increases, providing an appreciable entropic contribution to the Gibbs energy at the synthesis temperature and, in turn, explaining the influence of Ge_f on the degree of structural order. The most stable HPM-18 polymorph is E.

Author contributions

HY: conceptualization, supporting; methodology, supporting; validation, lead; formal analysis, lead; investigation, lead; data curation, lead; writing – original draft, supporting; writing – review & editing, supporting. ZZ: validation, lead; formal analysis, supporting; investigation, supporting; data curation, lead; writing – review & editing, supporting. JL: methodology, supporting; validation, supporting; formal analysis, supporting; investigation, supporting; resources, supporting; writing – original draft, supporting; writing – review & editing, lead; funding acquisition, supporting. SRGB: software, lead; validation, lead; formal analysis, supporting; investigation, supporting; resources, supporting; data curation, supporting; writing – original draft, supporting; writing – review & editing, lead; visualization, supporting; funding acquisition, supporting. ZRG: conceptualization, lead; methodology, lead; investigation, supporting; data curation, supporting; writing – original draft, supporting; writing – review & editing, lead; visualization, lead; supervision, supporting; project administration, lead. MAC: conceptualization, lead; methodology, lead; investigation, supporting; resources, lead; data curation, supporting; writing – original draft, lead; writing – review & editing, lead; supervision, lead; project administration, lead; funding acquisition, lead.

Conflicts of interest

There are no conflicts to declare.

Data availability

CCDC 2473072 (Experimental Crystal Structure Determination by cRED) and CCDC 2476607 (Experimental Rietveld refined structure) contain the supplementary crystallographic data for this paper.[55a,b]

Other data for this article, including multinuclear MAS NMR, XRD and calculated energy data are available at ZENODO at https://doi.org/10.5281/zenodo.16949065.

Supplementary information (SI): the authors have cited additional references within the SI.[49–54] The experimental section, tables of synthesis results, crystallographic data, enumeration of HPM-18 polymorphs, and cRED, PXRD and FESEM images. See DOI: https://doi.org/10.1039/d5ta06932g.

Acknowledgements

Financial support from the Spanish Ministry of Science and Innovation (PID2022-137889OB-I00, TED2021-131223B-I00, and MCIN/AEI/10.13039/501100011033) is gratefully acknowledged. Synchrotron powder X-ray diffraction experiments were performed at the Materials Science Powder Diffraction beamline bl04 at the ALBA Spanish Synchrotron with the collaboration of the ALBA staff. H. Y. is grateful to the China Scholarship Council for a PhD grant. S. R. G. B. acknowledges grant RYC2022-036070-I funded by MICIU/AEI/10.13039/501100011033 and by "ESF+". The authors would like to acknowledge the computing time provided by the Servicio de Supercomputación de la Universidad de Granada. We acknowledge the Severo Ochoa Centres of Excellence program through Grant CEX2024-001445 S.

Notes and references

1 H. Zhang, I. bin Samsudin, S. Jaenicke and G.-K. Chuah, Zeolites in Catalysis: Sustainable Synthesis and Its Impact on Properties and Applications, *Catal. Sci. Technol.*, 2022, **12**(19), 6024–6039.
2 K. Chen, S. H. Mousavi, R. Singh, R. Q. Snurr, G. Li and P. A. Webley, Gating Effect for Gas Adsorption in Microporous Materials—Mechanisms and Applications, *Chem. Soc. Rev.*, 2022, **51**(3), 1139–1166.
3 E. Koohsaryan, M. Anbia and M. Maghsoodlu, Application of Zeolites as Non-phosphate Detergent Builders: A Review, *J. Envir. Chem. Eng.*, 2020, **8**(5), 104287.
4 T. F. Degnan, Applications of Zeolites in Petroleum Refining, *Top. Catal.*, 2000, **13**(4), 349–356.
5 X. Han, W. Xu, F. Meng, Z. Liu and C. Liao, Recent Advances in Zeolite Membranes for Gas Separation and Pervaporation in Petrochemicals, *J. Mater. Chem. A*, 2025, **13**, 10358–10387.
6 I. Kabalan, B. Lebeau, H. Nouali, J. Toufaily, T. Hamieh, B. Koubaissy, J. P. Bellat and T. J. Daou, New Generation of Zeolite Materials for Environmental Applications, *J. Phys. Chem. C*, 2016, **120**(5), 2688–2697.
7 Y. Li, L. Li and J. Yu, Applications of Zeolites in Sustainable Chemistry, *Chem*, 2017, **3**(6), 928–949.
8 D. Kalló, Applications of Natural Zeolites in Water and Wastewater Treatment, *Rev. Miner Geochem.*, 2001, **45**, 519–550.
9 L. Gómez-Hortigüela and M. A. Camblor, in *In Insights into the Chemistry of Organic Structure-Directing Agents in the Synthesis of Zeolitic Materials*, ed. L. Gómez-Hortigüela, Springer International Publishing, Cham, 2018, pp 1–41.
10 M. E. Davis and R. F. Lobo, Zeolite and Molecular Sieve Synthesis, *Chem. Mater.*, 1992, **4**(4), 756–768.
11 A. W. Burton, S. I. Zones and S. Elomari, The Chemistry of Phase Selectivity in the Synthesis of High-Silica Zeolites, *Curr. Opin. Colloid Interface Sci.*, 2005, **10**(5), 211–219.
12 M. A. Camblor and S. B. Hong, Synthetic Silicate Zeolites: Diverse Materials Accessible Through Geoinspirationin Porous Materials, in *Inorganic Materials Series*, ed D. W. Bruce, D. O'Hare, R. I. Walton, Wiley, Chichester, 2011, pp 265–325.
13 T. Blasco, A. Corma, M. J. Díaz-Cabañas, F. Rey, J. A. Vidal-Moya and C. M. Zicovich-Wilson, Preferential Location of Ge in the Double Four-Membered Ring Units of ITQ-7 Zeolite, *J. Phys. Chem. B*, 2002, **106**(10), 2634–2642.
14 M. Camblor, L. Villaescusa and M. Diaz-Cabanas, Synthesis of All-Silica and High-Silica Molecular Sieves in Fluoride Media, *Top. Catal.*, 1999, **9**, 59–76.
15 M. Camblor, P. Barrett, M. Diaz-Cabanas, L. Villaescusa, M. Puche, T. Boix, E. Perez and H. Koller, High Silica Zeolites with Three-Dimensional Systems of Large Pore Channels, *Microporous Mesoporous Mater.*, 2001, **48**, 11–22.
16 C. M. Zicovich-Wilson, M. L. San-Roman, M. A. Camblor, F. Pascale and J. S. Durand-Niconoff, Structure, Vibrational Analysis, and Insights into Host-Guest Interactions in As-Synthesized Pure Silica ITQ-12 Zeolite by Periodic B3LYP Calculations, *J. Am. Chem. Soc.*, 2007, **129**(37), 11512–11523.
17 A. Rojas, E. Martinez-Morales, C. M. Zicovich-Wilson and M. A. Camblor, Zeolite Synthesis in Fluoride Media: Structure Direction toward ITW by Small Methylimidazolium Cations, *J. Am. Chem. Soc.*, 2012, **134**(4), 2255–2263.
18 L. Villaescusa, P. Barrett and M. A. Camblor, Calcination of Octadecasil: Fluoride Removal and Symmetry of the Pure SiO2 Host, *Chem. Mater.*, 1998, **10**(12), 3966–3973.
19 C. M. Zicovich-Wilson, M. L. San Román and A. Ramírez-Solís, Mechanism of F- Elimination from Zeolitic D4R Units: A Periodic B3LYP Study on the Octadecasil Zeolite, *J. Phys. Chem. C*, 2010, **114**(7), 2989–2995.
20 W. J. Roth, P. Nachtigall, R. E. Morris, P. S. Wheatley, V. R. Seymour, S. E. Ashbrook, P. Chlubná, L. Grajciar, M. Položij, A. Zukal, O. Shvets and J. Čejka, A Family of Zeolites with Controlled Pore Size Prepared Using a Top-down Method, *Nat. Chem.*, 2013, **5**, 628–633.
21 P. Eliášová, M. Opanasenko, P. S. Wheatley, M. Shamzhy, M. Mazur, P. Nachtigall, W. J. Roth, R. E. Morris and J. Čejka, The ADOR Mechanism for the Synthesis of New Zeolites, *Chem. Soc. Rev.*, 2015, **44**(20), 7177–7206.
22 O. Veselý, R. E. Morris and J. Čejka, Beyond Traditional Synthesis of Zeolites: The Impact of Germanosilicate Chemistry in the Search for New Materials, *Microporous Mesoporous Mater.*, 2023, **358**, 112385.
23 M. Mazur, P. S. Wheatley, M. Navarro, W. J. Roth, M. Položij, A. Mayoral, P. Eliášová, P. Nachtigall, J. Čejka and R. E. Morris, Synthesis of "unfeasible" Zeolites, *Nat. Chem.*, 2016, **8**, 58–62.
24 F. Daeyaert and M. Deem, De Novo Design of Organic Structure Directing Agents for the Synthesis of Zeolites. In *AI-Guided Design and Property Prediction for Zeolites and Nanoporous Materials*, John Wiley & Sons, Ltd, 2023, pp 33–59.
25 L. Burel, N. Kasian and A. Tuel, Quasi All-Silica Zeolite Obtained by Isomorphous Degermanation of an As-Made Germanium-Containing Precursor, *Angew. Chem., Int. Ed.*, 2014, **53**(5), 1360–1363.
26 H. Xu, J. Jiang, B. Yang, L. Zhang, M. He and P. Wu, Post-Synthesis Treatment Gives Highly Stable Siliceous Zeolites through the Isomorphous Substitution of Silicon for Germanium in Germanosilicates, *Angew. Chem., Int. Ed.*, 2014, **53**, 1355–1359.
27 M. V. Shamzhy, P. Eliasová, D. Vitvarova, M. V. Opanasenko, D. S. Firth and R. E. Morris, Post-Synthesis Stabilization of Germanosilicate Zeolites ITH, IWW, and UTL by Substitution of Ge for Al, *Chem.–Eur. J.*, 2016, **22**(48), 17377–17386.
28 X. Yang, M. A. Camblor, Y. Lee, H. Liu and D. Olson, Synthesis and Crystal Structure of As-Synthesized and Calcined Pure Silica Zeolite ITQ-12, *J. Am. Chem. Soc.*, 2004, **126**(33), 10403–10409.
29 A. Rojas and M. A. Camblor, A Pure Silica Chiral Polymorph with Helical Pores, *Angew. Chem., Int. Ed.*, 2012, **51**, 3854–3856.

30 R. T. Rigo, S. R. G. Balestra, S. Hamad, R. Bueno-Perez, A. R. Ruiz-Salvador, S. Calero and M. A. Camblor, The Si-Ge Substitutional Series in the Chiral STW Zeolite Structure Type, *J. Mater. Chem. A*, 2018, **6**(31), 15110–15122.

31 Y. Wang, J. Song and H. Gies, The Substitution of Germanium for Silicon in AST-Type Zeolite, *Solid State Sci.*, 2003, **5**, 1421–1433.

32 P. Barrett, T. Boix, M. Puche, D. Olson, E. Jordan, H. Koller and M. A. Camblor, ITQ-12: A New Microporous Silica Polymorph Potentially Useful for Light Hydrocarbon Separations, *Chem. Comm.*, 2003, **17**, 2114–2115.

33 M. A. Camblor, M. Diaz-Cabanas, J. Perez-Pariente, S. Teat, W. Clegg, I. Shannon, P. Lightfoot, P. Wright and R. E. Morris, SSZ-23: An Odd Zeolite with Pore Openings of Seven and Nine Tetrahedral Atoms, *Angew. Chem., Int. Ed.*, 1998, **37**, 2122–2126.

34 Ch. Baerlocher, D. Brouwer, B. Marler and L. B. McCusker, Database of Zeolite Structures, can be found under https://www.iza-structure.org/databases/, 2025, accessed: 20/05/2025.

35 S. C. Weston, B. K. Peterson, J. E. Gatt, W. W. Lonergan, H. B. Vroman, M. Afeworki, G. J. Kennedy, D. L. Dorset, M. D. Shannon and K. G. Strohmaier, EMM-17, a New Three-Dimensional Zeolite with Unique 11-Ring Channels and Superior Catalytic Isomerization Performance, *J. Am. Chem. Soc.*, 2019, **141**(40), 15910–15920.

36 Z. R. Gao, J. Li, C. Lin, A. Mayoral, J. Sun and M. A. Camblor, HPM-14: A New Germanosilicate Zeolite with Interconnected Extra-Large Pores Plus Odd-Membered and Small Pores, *Angew. Chem., Int. Ed.*, 2021, **60**, 3438–3442.

37 C. M. Zicovich-Wilson, F. Gandara, A. Monge and M. A. Camblor, In Situ Transformation of TON Silica Zeolite into the Less Dense ITW: Structure-Direction Overcoming Framework Instability in the Synthesis of SiO2 Zeolites, *J. Am. Chem. Soc.*, 2010, **132**(10), 3461–3471.

38 X. Wang, Y. Shen, R. Liu, X. Liu, C. Lin, D. Shi, Y. Chen, F. Liao, J. Lin and J. Sun, Elucidation of Correlated Disorder in Zeolite IM-18, *Act. Crystallogr. B*, 2019, **75**, 333–342.

39 P. Lu, L. A. Villaescusa and M. A. Camblor, Driving the Crystallization of Zeolites, *Chem. Rec.*, 2018, **18**, 713–723.

40 A. Coelho, TOPAS and TOPAS-Academic: an optimization program integrating computer algebra and crystallographic objects written in C++, *J. Appl. Crystallogr.*, 2018, **51**, 210–218.

41 C. Baerlocher, A. Hepp, W. M. Meier and M. W and DLS-76, *A Program for the Simulation of Crystal Structures by Geometric Refinement. Institute of Crystallography and Petrography*, ETH Zurich, Zurich (Switzerland), 1976.

42 "Topas wiki" can be found under***https://topas.awh.durham.ac.uk/doku.php?id=anisotropic_hkl***, 2025, accessed: 20/03/25.

43 Deposition number 2476607 (for ordered HPM-18) contains the supplementary crystallographic data for this paper. These data are provided free of charge by the joint Cambridge Crystallographic Data Centre and Fachinformationszentrum Karlsruhe Access Structures service.

44 M. O. Cichocka, Y. Lorgouilloux, S. Smeets, J. Su, W. Wan, P. Caullet, N. Bats, L. B. McCusker, J.-L. Paillaud and X. Zou, Multidimensional Disorder in Zeolite IM-18 Revealed by Combining Transmission Electron Microscopy and X-Ray Powder Diffraction Analyses, *Cryst. Growth Des.*, 2018, **18**(4), 2441–2451.

45 J. H. Kang, D. Xie, S. I. Zones, S. Smeets, L. B. McCusker and M. E. Davis, Synthesis and Characterization of CIT-13, a Germanosilicate Molecular Sieve with Extra-Large Pore Openings, *Chem. Mater.*, 2016, **28**, 6250–6259.

46 Z.-H. Gao, F.-J. Chen, L. Xu, L. Sun, Y. Xu and H.-B. Du, A Stable Extra-Large-Pore Zeolite with Intersecting 14- and 10-Membered-Ring Channels, *Chem.–Eur. J.*, 2016, **22**, 14367–14372.

47 L. Xu, L. Zhang, J. Li, K. Muraoka, F. Peng, H. Xu, C. Lin, Z. Gao, J.-G. Jiang, W. Chaikittisilp, J. Sun, T. Okubo and P. Wu, Crystallization of a Novel Germanosilicate ECNU-16 Provides Insights into the Space-Filling Effect on Zeolite Crystal Symmetry, *Chem.–Eur. J.*, 2018, **24**, 9247–9253.

48 "Intergrowth Family IM-18" can be found underhttps://america.iza-structure.org/IZA-SC/DO_structures/DO_family_scu.php?ID=14, 2025, accessed: 02/07/2025.

49 J. D. Gale, GULP: A computer program for the symmetry-adapted simulation of solids, *J. Chem. Soc., Faraday Trans.* 1997, 93, 629–637–.

50 J. D. Gale and A. L. Rohl, The General Utility Lattice Program (GULP), *Mol. Simul.*, 2003, 29, 291–341–.

51 G. S. J. Gale, Derivation of an Interatomic Potential for Fluoride-Containing Microporous Silicates and Germanates, *Chem. Mater.*, 2005, 17, 4, 730–740–.

52 R. Grau-Crespo, S. Hamad, C. R. A. Catlow and N. H. de Leeuw, Symmetry-adapted configurational modelling of fractional site occupancy in solids, *J. Phys. Condens. Matter* 2007, 19, 256201.

53 R. Grau-Crespo and U. V. Waghmare in *Molecular Modeling for the Design of Novel Performance Chemicals and Materials*, ed. B. Rai, CRC Press, 2012, ch. 11.

54 J. Arce-Molina, R. Grau-Crespo, D. W. Lewis, A. R. Ruiz-Salvador, Screening heteroatom distributions in zeotype materials using an effective Hamiltonian approach: the case of aluminogermanate PKU-9, *Phys. Chem. Chem. Phys.*, 2018, 20, 18047–18055–.

55 (*a*) CCDC 2473072: Experimental Crystal Structure Determination, 2025, DOI: 10.5517/ccdc.csd.cc2p0fjp; (*b*) CCDC 2476607: Experimental Crystal Structure Determination, 2025, DOI: 10.5517/ccdc.csd.cc2p43kj.